Journal of King Saud University – Science 34 (2022) 101807

Contents lists available at ScienceDirect

Journal of King Saud University – Science

journal homepage: www.sciencedirect.com

Original article

Self-assembly of a new cobalt complex, $(C_6H_{14}N_2)_3[CoCl_4]Cl$: Synthesis, empirical and DFT calculations

Mariem Tahenti [a], Noureddine Issaoui [b,*], Thierry Roisnel [c], Houda Marouani [a], Omar Al-Dossary [d], Aleksandr S. Kazachenko [e,f]

[a] University of Carthage, Faculty of Sciences of Bizerte, Laboratory of Material Chemistry (LR13ES08), 7021 Bizerte, Tunisia
[b] University of Monastir, Faculty of Sciences, Laboratory of Quantum and Statistical Physics (LR18ES18), Monastir 5079, Tunisia
[c] Univ Rennes, CNRS, ISCR (Institut des Sciences Chimiques de Rennes) - UMR 6226, F-35000 Rennes, France
[d] Department of Physics and Astronomy, College of Science, King Saud University, PO Box 2455, Riyadh 11451, Saudi Arabia
[e] Siberian Federal University, pr. Svobodny, 79, 660041Krasnoyarsk, Russia
[f] Institute of Chemistry and Chemical Technology, Krasnoyarsk Science Center, Siberian Branch, Russian Academy of Sciences, Akademgorodok, 50/24, 660036 Krasnoyarsk, Russia

ARTICLE INFO

Article history:
Received 2 September 2021
Revised 1 November 2021
Accepted 27 December 2021
Available online 31 December 2021

Keywords:
Hirshfeld surfaces
ELF
AIM
RDG
NCI

ABSTRACT

The aim of this work is the preparation and the crystallization of new organic–inorganic hybrid compound including cyclohexylamine and $[CoCl_4]^{2-}$, $(C_6H_{14}N_2)_3[CoCl_4]Cl$. Our compound has been studied by single-crystal X-ray diffraction (XRD), IR and TG-DTA examination. The XRD investigation allows to structurally distinguish our material by its monoclinic system and $P2_1/n$ space group through the lattice parameters a = 15.2645 (12) Å, b = 10.0843 (7) Å, c = 17.4450 (13) Å, β = 95.957 (3)° and Z = 4. The crystal arrangement shows inorganic entities of $[CoCl_4]^{2-}$ and chloride spreading in (10 $\bar{1}$) plane which are connected to cyclohexylammonium cations via N(C)–H...Cl H-bonds. The experimental studies on the compound have been accompanied computationally by DFT calculations *via* the B3LYP functional. The intermolecular interactions using were quantitatively studied by 3D-HS coupled with two dimensional fingerprint (2D-FP) plots and analyzed by the RDG and AIM approaches. The electron localization function (ELF) investigation was performed to explain the chemical structure of $(C_6H_{14}N_2)_3[CoCl_4]Cl$.
© 2021 The Author(s). Published by Elsevier B.V. on behalf of King Saud University. This is an open access article under the CC BY-NC-ND license (http://creativecommons.org/licenses/by-nc-nd/4.0/).

1. Introduction

Hybrid materials associated in different areas of research such as physics, biology and chemistry have been widely explored in recent years as new generation of high performance materials in chemical research along several years. To study the properties of those compounds many field of applications have been investigate including catalytic, magnetic, electrical conductivity, biochemistry, photochemistry and medicine (Jomaa et al., 2020; Novena et al., 2016; Gatfaoui et al., 2020; Daghar et al., 2022). Thus, the organic moieties have been based on physical and electronic proprieties, which providing to original optical attitude (Jiang et al., 2010). Cyclohexylamine and its derivatives have been of significant interest owing to their reagent for metal ions, which have reactivity and adaptability ensured the stabilization of sundry structures (Yun et al., 2004). This organic molecule can be associated to inorganic moiety by hydrogen bond interaction inside the structure N(C)–H...X in order to assemble and offer the crystal organization network of hybrid matter for structural examination. Hybrid compounds of the A_2MX_4 crystal family attract a current attention in the area of chemistry because of their magnetic (Chen et al., 2012) and thermal (Chang et al., 2011) behaviors which can be correlated to interionic lengths between the $[MX_4]^{2-}$ anions and the connections involving the ions. The modification of the metal ion can concern the shape of MX_4^{2-} and, therefore, changes both the structure of the crystal and the type of the connections in the compound. In this context, organic–inorganic material template on transition metal cobalt(II) halide with tetrahedral (Moutia et al., 2016) or octahedral (Essid et al., 2015) coordination has been one of the recent interest researches. Therefore, hybrid compounds based on Co(II) halide containing CoX_4 tetrahedral anions; display several phase transitions assigned to the substituted amino group

* Corresponding author.
E-mail addresses: issaoui_noureddine@yahoo.fr (N. Issaoui), omar@ksu.edu.sa (O. Al-Dossary).
Peer review under responsibility of King Saud University.

Production and hosting by Elsevier

https://doi.org/10.1016/j.jksus.2021.101807
1018-3647/© 2021 The Author(s). Published by Elsevier B.V. on behalf of King Saud University.
This is an open access article under the CC BY-NC-ND license (http://creativecommons.org/licenses/by-nc-nd/4.0/).

reorientation dynamics. An interesting study of this type is due to the fact they provide the numerous physic-chemical properties, conducting to various applications in optical (Abkari et al., 2017) and antimicrobial (Zheng et al., 2012) fields. Consequently, the aim of this studies reported here is to focus on the $(C_6H_{14}N)_3[CoCl_4]Cl$ compound, synthesis, XRD study, Hirshfeld analysis, vibrational spectroscopy, spectroscopic measurement (absorption) and thermal survey which was analyzed by TG-DTA technique are devoted and discussed and have been as well combined with theoretical calculations results in which AIM, RDG, ESP, ELF, HOMO-LUMO orbital analyses have been calculated and performed by the DFT/ B3LYP/6-311 + G(d,p) method.

2. Experimental methods

2.1. Materials and chemical synthesis

The monocrystal of the title complex $(C_6H_{14}N)_3[CoCl_4]Cl$ was synthesized by adding a mixture of $CoCl_2{\cdot}6H_2O$ (0.24 g) and a few drops of HCl (37%) to the ethanol solution of cyclohexylamine (0.34 mL) (pH < 2.5). The mixture is left under magnetic stirring of 1 h hour and a half to stand in the open air. Few weeks later with slow evaporation in ambient temperature, green blue prismatic crystal was appeared and carefully selected with sufficient size of the crystals. All materials used products and solvents were commercially obtained from Sigma Aldrich Company.

2.2. XRD data collection and physical measurements

A monocrystal of sizes (0.48 × 0.32 × 0.18 mm) was selected for the crystallography analysis to the X-ray data by using Bruker-AXS APEXII diffractometer at 150 K employing monochromated MoKα radiation (λ = 0.71073 Å). Absorption improvements were effectuated using multi-scan approach with the SADABS strategy (Bruker, 2006). Amid 24,384 measured reflections we find that 6103 are independent and 4718 with intensity I > 2σ (I) on the range (2.3°-27.5°). The structure was developed in $P2_1/n$ space group and resolved by the direct method using the SHELXT-97 program package (Sheldrick, 2015a) and refined by SHELXL (Sheldrick, 2015b) through the WINGX program (Farrugia, 2012). The DIAMOND program (Brandenburg, 1998) allows the plot of the molecular structure. Finishing enhancement on F^2 merged at R $(F^2) = 0.032$ and $wR(F^2) = 0.071$. The features used for the XRD data assortment evenly the plan for the crystal structure investigation and its results are included in Table S1. The asymmetric unit with an ORTEP drawing of $(C_6H_{14}N)_3[CoCl_4]Cl$ is given in Fig. 1a.

The infrared spectrum was reported at RT among 4000–400 cm^{-1} with a Perkin-Elmer FT-IR 1000 spectrometer scattered with dried KBr and pressed to pellets. TG /DTA analysis was investigated by a multimodule 92 Setaram analyzer using in the range of RT to 880 K at a heating speed of 5 K min^{-1} and a simple mass of 10.9 mg.

2.3. Computational investigations

The Gaussian 09 program (Frisch et al., 2009) was used to achieve the optimization geometry and all the theoretical calculations by the DFT/B3LYP (Becke, 1993), the 6-311++G(d,p) basis set was adopted for all atoms except the metal, the LANL2DZ basis set and effective core potentials (ECPs) have been used in order to represent the Co atom. The vibrational assignments were carried out using the VEDA4 program (Jamróz, 2004). To understanding the intermolecular interactions we use the Crystal Explorer 3.1 package (Wolff et al., 2013) imported on a CIF file to generate 3D-HS and their related 2D-FP. To establish the topological analysis of non-covalent interaction we can utilize Multiwfn package (Lu and Chen, 2012), using Bader's theory (Kumar et al., 2016), while the RDG of the compound are mapped by Multiwfn and VMD programs (Humphrey et al., 1996). HOMO-LUMO distributions and ESP and ELF analysis were performed by the optimized molecular structure.

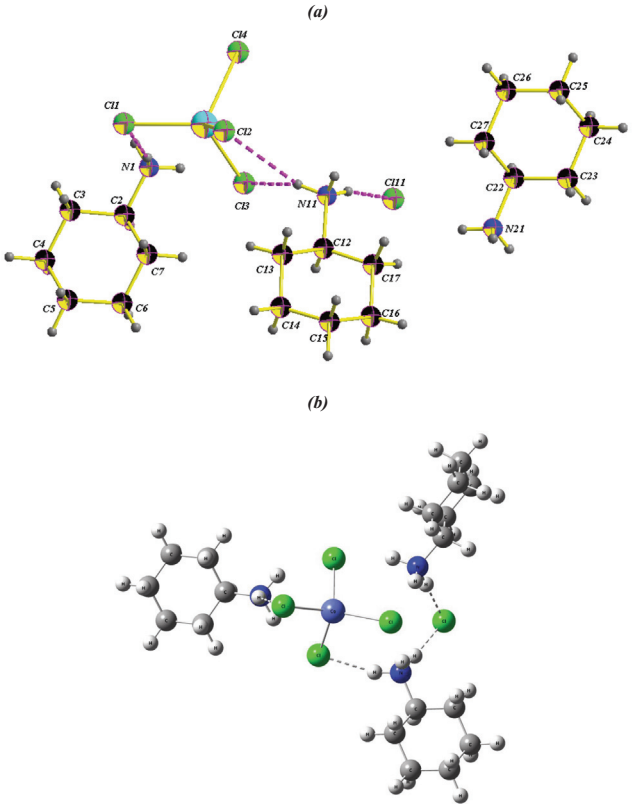

Fig. 1. Ortep structure (a) with atom numbering and optimized molecular geometrical structure (b) of $(C_6H_{14}N)_3[CoCl_4]Cl$.

3. Result and discussion

3.1. XRD and molecular modeling

To study the geometrical and optimized structure, the title compound was investigated by XRD analysis. To establish the structural model of $(C_6H_{14}N_2)_3[CoCl_4]Cl$, an ORTEP drawing (Fig. 1a) was designed by the asymmetric unit whose contain three cyclohexylammonium organic cations $(C_6H_{11}N_3^+)$, an anionic entity which is $[CoCl_4]^{2-}$ and an isolated Cl^- anion. The existence of free inorganic anions as a part of an anionic sublattice in hybrid compounds was also found in other structure (Ferchichi et al., 2010). The optimized geometric model of the structure is shown in Fig. 1b and Table 1 exhibits a comparison between experimental and calculated X-ray crystallographic parameters. The interatomic distances and the bonding angles of organic entity are in a good agreement with those crystallizing with other types of anion found in previous literature (Jomaa et al, 2021; Daghar et al. 2021).

The cyclohexylammonium cations adopt chair organization with an ammonium group in the equatorial position, with C–C average bond lengths equal to 1.520 Å and $d_{N\text{-}C}$ varying from 1.492 to 1.502 Å. The average differences between the calculated geometric parameters and those of the experimental parameters were found to be approximately 0.02 Å for C–N bond lengths while for C–C bonds is approximately 0.025 Å. Besides, the bond angles

Table 1
Principal intermolecular optimized and experimental bond lengths and bond angles (Å, °) parameters of $(C_6H_{14}N)_3[CoCl_4]Cl$ by X-ray data.

$[ClO_4]^-$					
Bond length (Å)			Bond angles (°)		
	RX	Cal.		RX	Cal.
Co–Cl1	2.2675 (5)	2.316	Cl1–Co–Cl2	118.32(2)	129.26
Co–Cl2	2.2605 (5)	2.400	Cl1–Co–Cl3	109.82(2)	103.61
Co–Cl3	2.2692 (5)	2.363	Cl1–Co–Cl4	106.94(2)	103.8
Co–Cl4	2.3081 (6)	2.408	Cl2–Co–Cl3	109.65(2)	106.86
Cl1–Cl2	3.8872 (2)	3.711	Cl2–Co–Cl4	107.16(2)	107.19
Cl1–Cl3	3.7120 (2)	4.227	Cl3–Co–Cl4	103.92(2)	103.52
Cl1–Cl4	3.6775 (2)	3.712			
Cl2–Cl3	3.7035 (2)	3.833			
Cl2–Cl4	3.6770 (2)	3.775			
Cl3–Cl4	3.6064 (3)	3.831			
Cation $C_6H_{11}NH_3^+$ (1)					
Bond length (Å)			Bond angles (°)		
	RX	Cal.		RX	Cal.
N1–C2	1.492 (3)	1.517	N1–C2–C3	110.08 (16)	109.87
C2–C3	1.511 (3)	1.542	N1–C2–C7	109.98 (16)	109.32
C2–C7	1.520 (3)	1.547	C2–C3–C4	110.16 (18)	110.39
C3–C4	1.531 (3)	1.546	C3–C2–C7	111.33 (17)	111.40
C4–C5	1.526 (4)	1.546	C5–C4–C3	111.4 (2)	111.44
C5–C6	1.510 (3)	1.547	C5–C6–C7	111.79 (18)	111.40
C6–C7	1.519 (3)	1.543	C6–C5–C4	111.2 (2)	111.41
C6–C7–C2	110.34 (18)	110.43			
Cation $C_6H_{11}NH_3^+$ (2)					
Bond length (Å)			Bond angles (°)		
	RX	Cal.		RX	Cal.
N11–C12	1.502 (2)	1.516	N11–C12–C13	109.38(15)	110.28
C12–C13	1.519 (3)	1.543	N11–C12–C17	108.91(16)	109.44
C12–C17	1.519 (3)	1.547	C13–C12–C17	113.50(16)	111.47
C13–C14	1.521 (3)	1.547	C14–C15–C16	111.23(17)	110.43
C14–C15	1.518 (3)	1.546	C15–C14–C13	110.41(18)	111.35
C15–C16	1.522 (3)	1.546	C15–C16–C17	111.37(16)	111.61
C16–C17	1.528 (3)	1.543			
Cation $C_6H_{11}NH_3^+$ (3)					
Bond length (Å)			Bond angles (°)		
	RX	Cal.		RX	Cal.
N21–C22	1.494 (2)	1.515	N21–C22–C27	109.72(15)	110.27
C22–C27	1.519 (2)	1.543	N21–C22–C23	109.46(15)	109.67
C22–C23	1.519 (3)	1.547	C27–C22–C23	111.81(16)	110.43
C23–C24	1.532 (3)	1.547	C22–C23–C24	110.53(17)	111.46
C24–C25	1.518 (3)	1.546	C25–C24–C23	112.11(18)	111.33
C25–C26	1.517 (3)	1.547	C26–C25–C24	111.11(18)	111.56
C26–C27	1.524 (3)	1.543	C25–C26–C27	110.53(17)	110.35
C22–C27–C26	110.81(16)	112.17			

(C–C–C) were observed by XRD between 110.16 and 113.50° and calculated between 110.39 and 112.17° and (N–C–C) observed by in the range of 109.58° and calculated at an average of 105.4°. The inorganic anion $[CoCl_4]^{2-}$ adopts a tetrahedral molecular geometry, a cobalt atom Co^{2+} in the center coordinated to four chlorine atoms at the corners of a tetrahedron with an sp^3 hybridization, with experimental and computed Co-Cl bond lengths ranging from 2.2605(5)–2.3081(6) Å and between 2.316 and 2.408 Å, respectively. The distinguished bond angles of Cl–Co–Cl varying from 103.92(2)° to 118.32(2)° for the experimental and from 103.52° to 129.26° for the theoretical calculations. The Cl…Cl distance among the two nearest neighbors $[CoCl_4]^{2-}$ tetrahedra is 4.128 Å. Furthermore, the halide-halide contacts are reputed to generate weak anti-ferromagnetic interactions that decrease rapidly with increasing Cl…Cl separation (Zhou et al., 1991). It's worth noting that these values (Table 1) are also found in other organic terachlorocobltate (Tahenti et al. 2020). This slight difference between observed and calculated parameters is due to the interatomic interactions in the crystalline state. Moreover, the τ_4 defined by Alvarez (Alvarez and Llunell, 2000) was an index parameter used for the four-coordinate transition metal complexes to explain the geometry of materials and defined by the sum of α and β angles the two biggest angles in the four-coordinate species, specified by this relation:

$$\tau = \frac{360^{\circ} - (\alpha + \beta)}{141^{\circ}}$$

Exercising this equation on $(C_6H_{14}N_2)_3[CoCl_4]Cl$ reveal an τ_4 equal to 0.935 which is close to 1, so we can highlight a slightly distorted tetrahedral geometry.

As we can see in Fig. 3a, the projection of the studied compound by the side of the $\vec{b}$ axis shows the atomic organization of all the species involved in the crystal. It exhibits the arrangement of the tetrachlorocobaltate and chloride anions in $(\bar{1}\ 01)$ planes which intercalated the cyclohexylammonium groups presented in the chair conformation. Indeed, the projection of a single layer along

the $\vec{a}$ axis (Fig. 2b), demonstrates that the tetrachlorocobaltate anions are located in planes y = ¼ and ¾. The packing for $(C_6H_{14}N_2)_3[CoCl_4]Cl$ and the junction of cationic to chlorine groups of anionic entities are ensured by electrostatic interactions as well as by hydrogen bonding which summarized in Table 2 through N(C)-H...Cl with donor–acceptor length ranging from 3.198(3) Å to 3.488(6) Å for $d_{N...Cl}$, forming $R_1^2(4)$ and $R_6^3(12)$ motifs (Fig. 2c) and $d_{C...Cl}$ present an average of 3.683 Å gives birth to graphs $6R_2^1$ graph (Fig. 2d).

3.2. 3D-HS analysis

The analysis of molecular crystal structures based on 3D-HS was used to study and quantify the sizes and shapes of compounds (Arulraj et al., 2020a,b, 2022), also to define the space occupied by a molecule and to explore the intermolecular contact. Fig. 3 shows the asymmetric unit (a), the Hirshfeld molecular surface mapped in d_{norm} (−0.480–1.090) (b) of $(C_6H_{14}N)_3[CoCl_4]Cl$. The different results concerning hydrogen bonds discussed in the structural part (X-ray diffraction study) are summarized in an efficient way on d_{norm} mapping. It is observed on this map several dark red circular spots due to the contribution of H...Cl/Cl...H contacts (39%) on the surface plots of Hirshfeld, these spots corresponding to the H-bonds N(C)-H...Cl. Other spots (blue and white) appear on this map and they relate to H...H contacts. The d_{norm} cartography represented in Fig. 3b gives a general outline on some hydrogen bonds which participate in the stability of our crystalline structure.

Fig. S1 illustrates the 2D-FP plots of the $(C_6H_{14}N)_3[CoCl_4]Cl$ compound. This distribution shows that the intermolecular contacts H...H occupy (59.7%) of the entire HS and these later are shown on the fingerprint plot ($d_e = d_i$ = 1.1 Å), this value is greater than the vdW radius of the hydrogen atom (1.09 Å). The H...Cl/Cl...H contacts represent almost 1/3 of the entire Hirshfeld surface. Indeed, the organic part has a great number of H atoms on their molecular surface (S_H = 79.45%), while the carbon atoms are hardly ever present on the surface of the molecule (S_C = 0%) as they usually form four bonds with other atoms (Fig. S2). The rest of the H...Co/Co...H and Cl...Cl contacts occupy 0.5% and 0.3% of the Hirshfeld surface, respectively. The identified intermolecular interactions were evaluated by analysis of enrichment ratios. The ratios are given in Table S2. The list of enrichment ratios highlights H...Cl/Cl...H contacts (ER_{HCl} = 1.24) which appear to be favored in crystal packaging with the formation of hydrogen bonds of type N–H...Cl and C–H...Cl. H... H contacts appear with an ER ratio nearly to unity (ER_{HH} = 0.95).

3.3. Vibrational spectroscopic study

The infrared absorption spectroscopy of our study compound has the role of determining the vibrational characteristics of atomic groups, as well the enumeration of the modes of vibration and the attribution of the bungs to the different types of vibratory movements in the anionic groups $[CoCl_4]^{2-}$. In addition, in our study, we performed a vibrational analysis of $(C_6H_{14}N)_3[CoCl_4]Cl$ using the experimental spectrum which was measured in the range of frequency 400–4000 cm^{-1} and theoretical one was performed using DFT/B3LYP/6–311 + G(d,p) basis set are shown in Fig. S3. The experimental IR wavenumber and the theoretical one from DFT conception were assigned by VEDA program (Jamróz, 2004) and GaussView package (Dennington et al., 2009). The different vibration bands existing in produced compound based on bibliographic data relating to the different types of bonds in the same organic molecule (Jomaa et al., 2021) as well as the tetrachlorocobaltate anion have been assigned to all bands appeared in the infrared spectrum. Theoretical calculation presents more

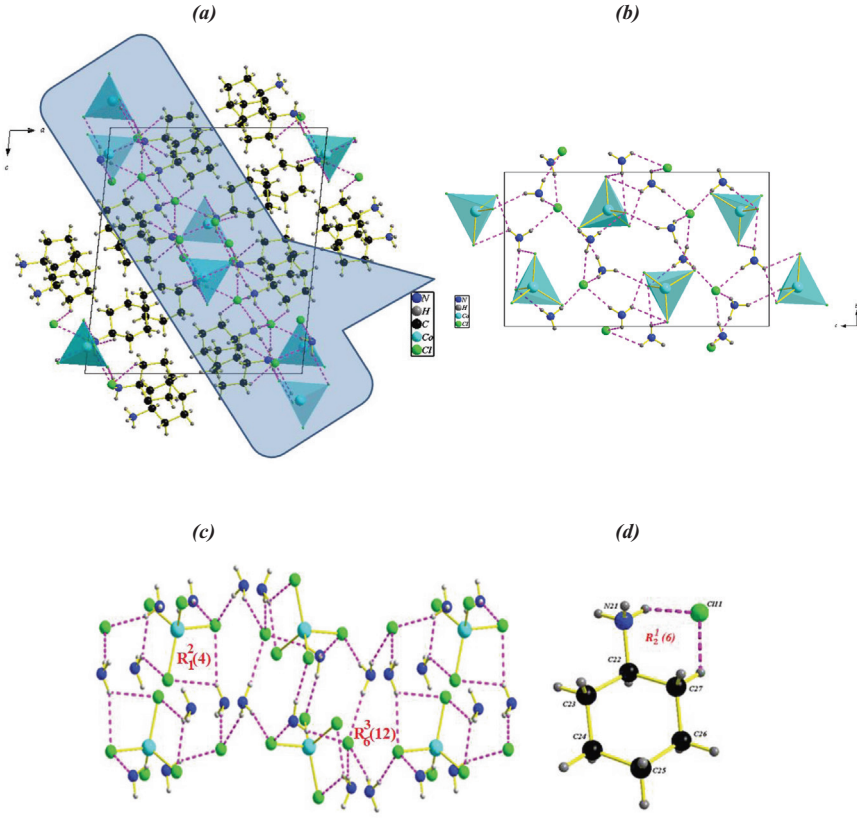

Fig. 2. The space filler of $(C_6H_{14}N)_3[CoCl_4]Cl$ viewed along the b-axis.

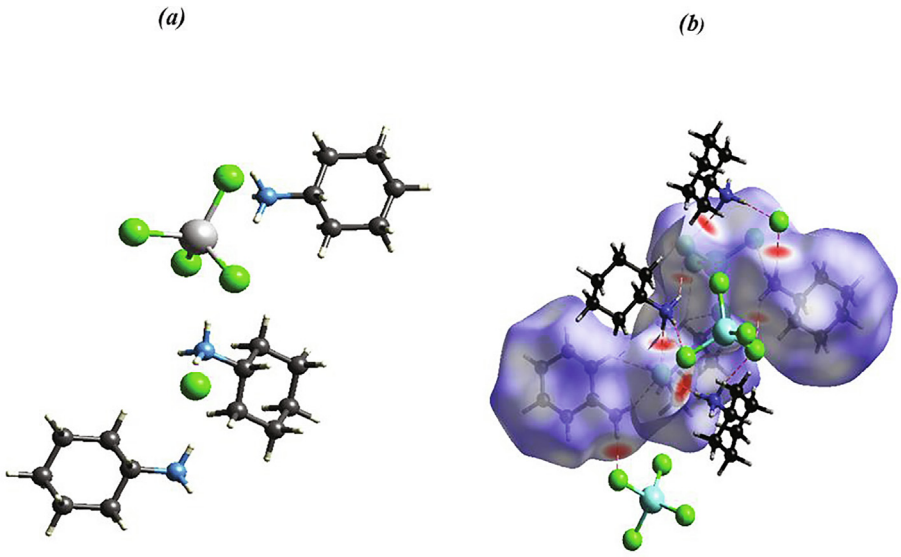

Fig. 3. The asymmetric unit (a), the Hirshfeld molecular surface mapped in d_{norm} (-0.480–1.090) (b) of $(C_6H_{14}N)_3[CoCl_4]Cl$.

Table 2
Hydrogen-bond geometry (Å, °) of $(C_6H_{14}N)_3[CoCl_4]Cl$.

D–H···A	D–H (Å)	H···A(Å)	D···A (Å)	D–H···A(°)
N1–H1A···Cl4^{i}	0.89 (2)	2.62 (2)	3.394 (4)	146.3 (2)
N1–H1B···Cl1	0.92 (2)	2.37 (2)	3.261 (2)	165.3 (2)
N1–H1C···Cl11^{i}	0.87 (2)	2.45 (2)	3.283 (4)	162.3 (2)
N11–H11A···Cl11	0.91 (2)	2.32 (2)	3.204 (2)	165.6(2)
N11–H11B...Cl4^{ii}	0.91 (2)	2.59(2)	3.427 (2)	154.1(2)
N11–H11B...Cl2^{ii}	0.91 (2)	2.81(2)	3.352 (3)	119.5(2)
N11–H11C···Cl2	0.91 (2)	2.87 (2)	3.488 (6)	126.5(2)
N11–H11C···Cl3	0.91 (2)	2.44 (2)	3.232 (2)	145.3 (2)
N21–H21A···Cl4^{iii}	0.88 (2)	2.39 (2)	3.251 (4)	168.6 (2)
N21–H21B···Cl11^{iv}	0.91 (2)	2.35 (2)	3.237 (2)	166.4 (2)
N21–H21C···Cl11^{v}	0.88 (2)	2.38 (2)	3.198 (3)	154.4 (2)
C2–H2···Cl2^{vi}	1.00	2.86	3.674 (2)	138.9
C13–H13B···Cl4^{ii}	0.99	2.89	3.718 (3)	141.9
C17–H17A···Cl4^{i}	0.99	2.85	3.693 (3)	143.3
C27–H27B···Cl11^{vii}	0.99	2.88	3.647 (2)	135.4

Symmetry codes:(i) −x + 1, −y + 1, −z + 1; .(ii) −x + 1, −y, 1 − z (iii) x + 1/2, −y + 1/2, z + 1/2; (iv) −x + 3/2, y−1/2, −z + 3/2; (v) −x + 3/2, y-1/2, z −3/2; (vi) x, 1 + y, z ; (vii) −x + 3/2, y + 1/2, −z + 1/2.

reasonable results from the point of view of number and positions of the bands because of the absence of imaginary frequencies. The assignments of the main groups are discussed below.

3.3.1. Vibrations of tetrachlorocobaltate(II) anion

Based on the work reported above and comparison with species containing these groups (Tahenti et al. 2020; Arulraj et al., 2020c), according to the DFT calculations, the various proposals for assignments of the vibration frequencies of $[CoCl_4]^{2-}$ anions are observed below 500 cm^{-1}. The stretching of Co-Cl observed at 107 and 132 cm^{-1}, respectively. The band, appeared in the 74 cm^{-1}, is attributed to the bending of this mode.

3.3.2. Vibrations of cyclohexylammonium cation

The high-frequency region between 3428 and 2854 cm^{-1} assigned to the stretching vibrations of the groups ($-NH_3^+$) and ($-CH_2$) of the organic entities, the widening of these bands is due to the establishment of the NCI type H-bonds. This later has an important effect of down shift the frequencies of these groupings. These bands appear in the range of 3643–3286 cm^{-1} in the theoretical IR spectrum (Daghar et al., 2021). Symmetrical and asymmetrical bending of the groups ($-NH_3^+$), and ($-CH_2$) and the stretching vibration C–C are located between 1578 and 1384 cm^{-1}, show good agreement with the previous studies (Jomaa et al., 2021) as well as DFT level. The band between 1116 and 1061 cm^{-1} can be recognized to the stretching vibration of the C-N group, almost the same values found in the theoretical spectrum in the region among 1186 and 1056 cm^{-1}. The bending modes of the C–N and C–C groups are predicted at 553 cm^{-1} and 442 cm^{-1}. This was computed to be found in the region 626–446 cm^{-1}. Based on these results, one can notice a good agreement between the computed and the experimental spectrum. The examinations of this figure show a small difference between the two IR spectra. This later is due to the fact that the experimental IR spectrum is recorded in the solid status, while the computed is performed for isolated molecules.

3.4. Thermal analysis

The differential thermal and thermogravimetric analysis of $(C_6H_{14}N)_3[CoCl_4]Cl$ is carried out under argon in the temperature range [307–580 K]. This analysis is carried out on 10.9 mg of the product placed in a platinum crucible with a heating rate of 5°. min^{-1}. DTA and TG diagrams are given in Fig. S4.

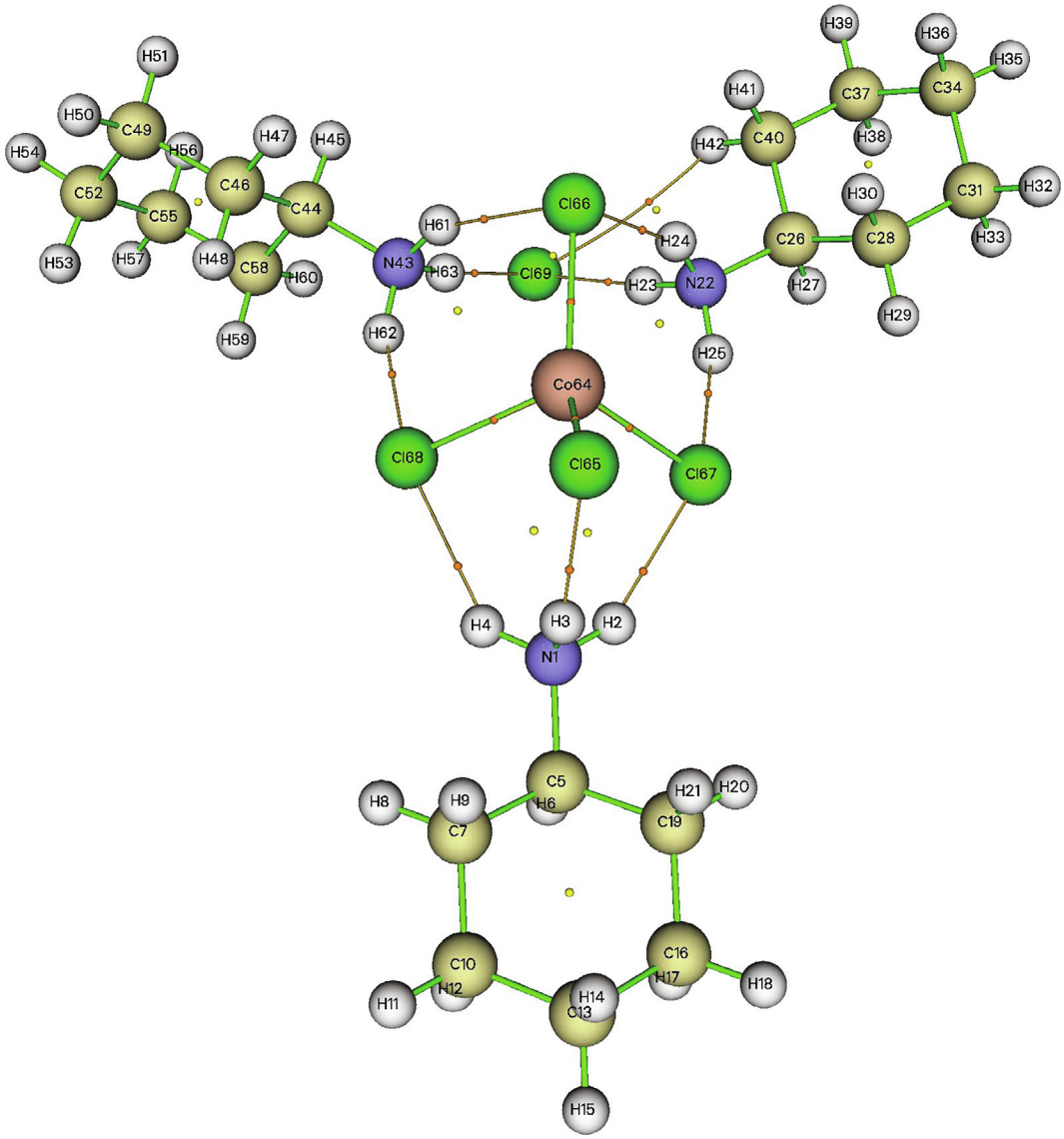

Fig. 4. AIM molecular diagram viewing the different BCPs of $(C_6H_{14}N)_3[CoCl_4]Cl$.

The DTA thermogram reveals that $(C_6H_{14}N)_3[CoCl_4]Cl$ undergoes a succession of endothermic peaks detected on the DTA diagram escorted by a loss of mass on the TG thermogram which can be endorsed to the pyrolysis of the cyclohexylamine entity. Then, an endothermic peak lacking loss of mass observed at 439 K which may match to a fusion. This observable fact is additional proved by heating $(C_6H_{14}N)_3[CoCl_4]Cl$ on a Kofler bench which makes it possible to approximate the material melting temperature, this 434 K temperature is nearly that inspected on the DTA bend (Gatfaoui S. et al., 2022). Lastly, an exothermic peak with loss of mass which appears at 498 K, it can match to the total decomposition of the organic molecule. Afterwards the residual product undertakes entire decomposition which guides to vaporous gas and black remains.

3.5. AIM topological analysis

Various theoretical investigations, particularly AIM (Atoms In Molecules) approach allows to distinguish the type and the stability of inter and intra-atomic interaction bonds, precisely the hydrogen bonds which is verified by the presence of the critical point (BCP), proposed by Bader's theory (Bader and Austen, 1997). Among the topological parameters we can found: the electron density ρ(r), the Laplacian $\nabla^2\rho(r)$, the eigenvalues (λ_1, λ_2, λ_3), the $\lambda1/\lambda3$ ratio, the kinetic energy densities G(r), the total energy densities H(r), the potential V(r) and the bond energy E offered several information on the properties of RCPs and BCPs of the title compound. Therefore, Multiwfn program (Lu and Chen, 2012) with LANL2DZ level is used to represent the AIM graphical analysis which is shown in Fig. 4 while the computed topological parameters of $(C_6H_{14}N)_3[CoCl_4]Cl$ are tabulated in Table 3.

As stated by Rozas et al. (Rozas et al., 2000), we can classify H-bonds to 3 classes: we have strong H-bonds when $\nabla^2\rho(r) < 0$ and the value of H(r) < 0, moderate H-bonds when $\nabla^2\rho(r) > 0$ and H(r) < 0 and weak H-bonds when $\nabla^2\rho(r) > 0$ and H(r) > 0.

Concerning Table 3 analysis, it can be observed that AIM analysis present 10H-bonds that meet up the Koch and Popelier criteria (Popelier et al., 2000) and that $Cl_{66}\ldots H_{24}$, $Cl_{67}\ldots H_2$, $Cl_{68}\ldots H_4$ and $Cl_{69}\ldots H_{23}$ interactions present symmetrical topological properties to $Cl_{66}\ldots H_{61}$, $Cl_{67}\ldots H_{25}$, $Cl_{68}\ldots H_{62}$ and $Cl_{69}\ldots H_{22}$ interactions. Also, the G/ρ ratio is used to distinguish the type of interaction which must be >1 to affirm the existence of H-bonds interactions. Positive

Table 3
AIM analysis of the bond critical points (BCP) for $(C_6H_{14}N)_3[CoCl_4]Cl$.

Bond critical points	Density of all electrons	Laplacian of electron density	Potential energy density V(r)	Energy density E(r) or H(r)	Interaction energy (E_{int}) kcal.mol^{-1}	Electron localization function (ELF)	Localized orbital locator (LOL)	Ellipticity	Eta index
$Cl_{67}...H_{25}$-N_{22}	0.02026	0.05760	−0.01416	0.00011	69.070	0.08383	0.23236	0.01505	0.21365
$Cl_{67}...H_{2}$-N_{1}	0.02262	0.06136	−0.01586	−0.00026	86.278	0.09967	0.24977	0.04965	0.22394
$Cl_{66}...H_{24}$-N_{22}	0.02176	0.05859	−0.01520	−0.00027	75.444	0.09615	0.24606	0.02001	0.22336
$Cl_{65}...H_{3}$-N_{1}	0.02518	0.06474	−0.01764	−0.00072	94.537	0.11876	0.26863	0.04935	0.23354
$Cl_{69}...H_{42}$-C_{40}	0.00521	0.01657	−0.00244	0.00085	−8.2300	0.18266	0.12035	1.41067	0.17371
$Cl_{69}.....H_{23}$-N_{22}	0.03972	0.08561	−0.02895	−0.00377	111.97	0.21748	0.34528	0.00775	0.27000
$Cl_{66}...H_{61}$-N_{43}	0.02167	0.05865	−0.01515	−0.00024	75.276	0.09510	0.24494	0.02170	0.22274
$Cl_{68}...H_{4}$-N_{1}	0.19386	0.05521	−0.01325	0.27518	73.681	0.08090	0.22893	0.07826	0.21312
$Cl_{69}...H_{63}$-N_{43}	0.04074	0.08747	−0.02980	−0.00396	115.12	0.22310	0.34900	0.00658	0.27146
$Cl_{68}.....H_{62}$-N_{43}	0.02033	0.05750	−0.01421	0.00008	68.283	0.08470	0.23337	0.01575	0.21432

Laplacian values are observed in the range of 0.01657 a.u and 0.08747 a.u at the CP of binding, is indicate that the distance between the interacting atoms is bigger than the sum of the vdW rays of these atoms, so is indicative of the existence of hydrogen weak bonds. This basis reveals that the title compound is stabilized by four Cl...H hydrogen bonds which are considered to be weak since the Laplacien and H(r) values are positive with bond energies in a range of −8.230 kcal mol^{-1} to 73.681 kcal mol^{-1}. While the moderate are located at the rest of H-bonds were confirmed by the negative value of the total energy densities H(r) with energy varying between 75.276 kcal mol^{-1} and 115.12 kcal mol^{-1}. These studies reveal clearly, that hydrogen bonds observed by XRD and HS analysis were investigated and confirmed by AIM approach.

3.6. RDG analysis

The non-covalent interaction (NCI) or RDG is a topological technique improved by Johnson et al. (2010) and Contreras-García et al. (2011) based on electronic density and used to examine the various types of interactions present in the title compound especially weak interactions like H-bond, vdW interaction and steric effect. This approach have been performed and mapped by VMD and Multiwfn softwares (Humphrey et al., 1996; Lu and Chen, 2012). From Fig. 5 we can distinguish the variation of RDG as a function of (ρ*sign λ_2). Generally, λ_2 is an essential parameter of the determination of the nature of interactions, it plays a very important role as indicator of stabilization or of destabilization of inter and intra interactions. As clearly seen in Fig. 6 significant by the evolution between RDG (a.u) versus sign (λ_2)ρ, which we employed a color code in order to indicate intensity and type bonds, sign (λ_2)ρ > 0 for repulsive interaction and characterized by red color spots, sign (λ_2)ρ < 0 for attractive interaction and have a blue color and sign (λ_2)ρ nearly zero for vdW interaction (weak interaction) described by green color. As we can see, the RDG peaks around −0.05, −0.02 u.a with sign (λ2)ρ correspond to a strong attractive NCI also by the low-density values (Akman F. et al., 2020). We can notice the light blue spots are located between the hydrogen and chlorine atoms, just to explain the strong attractive non covalent interaction type N–H...Cl. Also, green patches around the anion entity are accredited to vdW interactions. While the strong steric cyclic effect attached to repulsive interactions is associated by the elliptical red plaque situated at the center of the cycle.

3.7. Electrostatic surface potential (ESP)

ESP is an effective property for understanding reactivity in a molecule (A. Sagaama and N. Issaoui, 2020). This method allows the investigation of molecular interactions; it has been approved by the calculation of electrostatic properties derived from the charge density of a molecule (D. Romani et al., 2020). Fig. 7 indicates the electrostatic potential of our structure, the color of which depends on the value of ESP. The red color is specific for the negative electrostatic potential (chloride and the tetrachlorocobaltate anion), the yellow color slightly rich in electrons (nitrogen atoms) while the green color indicates where the potentials are close to zero and the blue color for the positive electrostatic potential.

It can be seen at the end that there is an overall electrostatic attraction between the cations and the anions.

3.8. ELF analysis

ELF is a new topological descriptor allows us to predict and understand the description of chemical structure (Sagaama A. et al., 2021). It makes possible to identify the nature of the weak interactions and the reactivity of the compound. Fig. 7 shows the ELF maps of $(C_6H_{14}N)_3[CoCl_4]Cl$, which characterized by two regions: regions of maximum Pauli repulsion (well-localized electrons), when ELF values close to 1 while the areas of minimum Pauli repulsion present an ELF values near 0 by using Multiwfn program (Lu and Chen, 2012). In addition, the blue color zone and especially dark blue areas located in the range (0–0.4) proved a reduction in ELF in the corresponding regions whereas the average ELF values appeared in the region of (0.5–0.8) are justified by color series goes from yellow to green. The higher first of the scale identified by the red color revealed a decrease in the ELF. The main conclusion that can be drawn from this part, ELF is related to the consequence of Pauli's repulsive effect (A. Sagaama and N. Issaoui, 2020). We can see that the strongest regions with maximum Pauli repulsion are represented by red area surrounded by single electron hydrogen atoms, while the regions characterized by the blue color are occupied by the chlorine atom of the tetrachlorocobaltate group and the carbon atoms of the organic entity allow us to understand that it belongs to the lowest regions with minimal Pauli repulsion.

3.9. Frontier molecular orbital analysis

The theoretical calculation was carried out using data from the CIF file studied using the DFT method. In the subject to study chemical reactivity and the stability and of the title compound, frontier molecular orbital (FMO) analyzes were investigated (Ghalla H. et al., 2014). The FMO orbitals of our studied compound are shown in Fig. S5. Examination of this figure shows clearly that HOMOs are located on the inorganic part of the crystal, while LUMOs are located on the organic part. The energy difference ΔE between two border orbitals is one of the first parameters to confirm the stability of our crystalline structure. The values of the HOMO and LUMO energies of our compound are −6.02 eV and

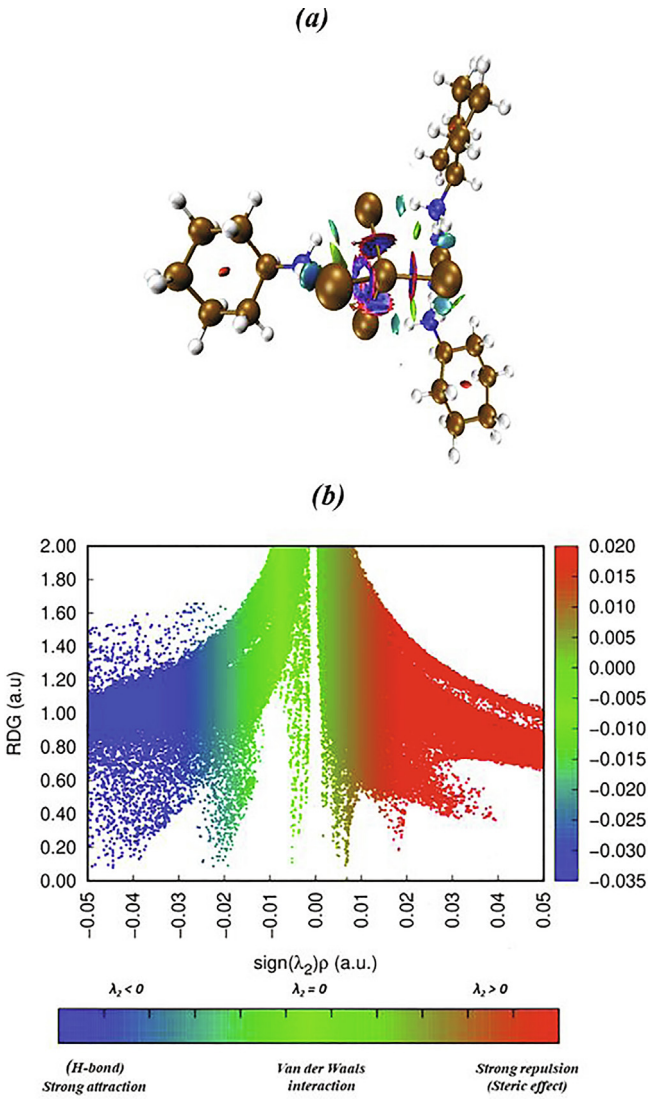

Fig. 5. Visualization of different interactions in $(C_6H_{14}N)_3[CoCl_4]Cl$ using Multiwfn and VMD softwares.

−3.45 eV respectively and other electronic properties electro negativity (χ), softness (S), etc..... are computed and grouped in Table S3. The band gap value is equal to Eg = 2.57 eV, close to 3 eV, this value implies that our prepared material behaves as a semiconductor, which is similar to other organic tetrachlorocobaltate(II) compounds (Tahenti et al., 2020).

To conclude, from the overhead parameters, we can notice that the gap energy of our studied compound is signed that is possessed a high kinetic stability (high-lying LUMO) and low reactivity criterion (low-lying HOMO).

4. Conclusion

This paper reveals the study and analysis of a new tetracholorocobaltate-based hybrid compound by several experimental and theoretical physiochemical methods. The structural analysis based on XRD found that H-bonding interactions N(C)-H...Cl have ensured the stabilization of the crystal, as well as investigated and examined by Hirshfeld Surface analysis. AIM, RDG and HOMO-LUMO theoretical approaches were performed to identify and to study the nature and the stability of different interactions. Furthermore, the vibrational properties of this com-

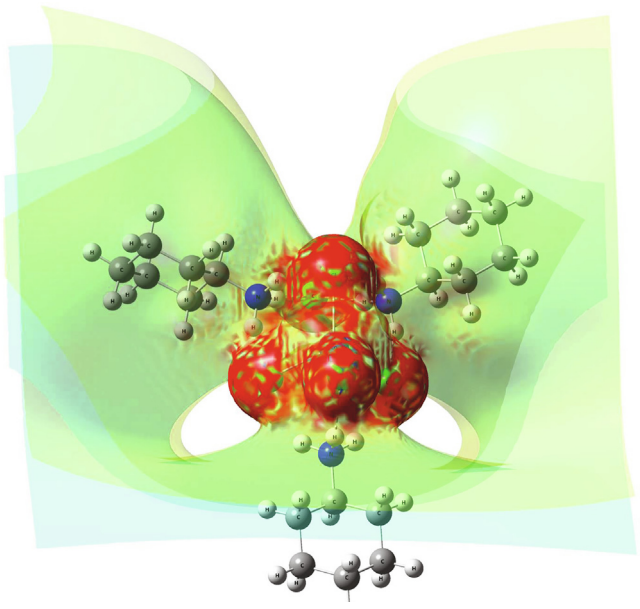

Fig. 6. Electrostatique Surface Potentiel (ESP) of $(C_6H_{14}N)_3[CoCl_4]Cl$.

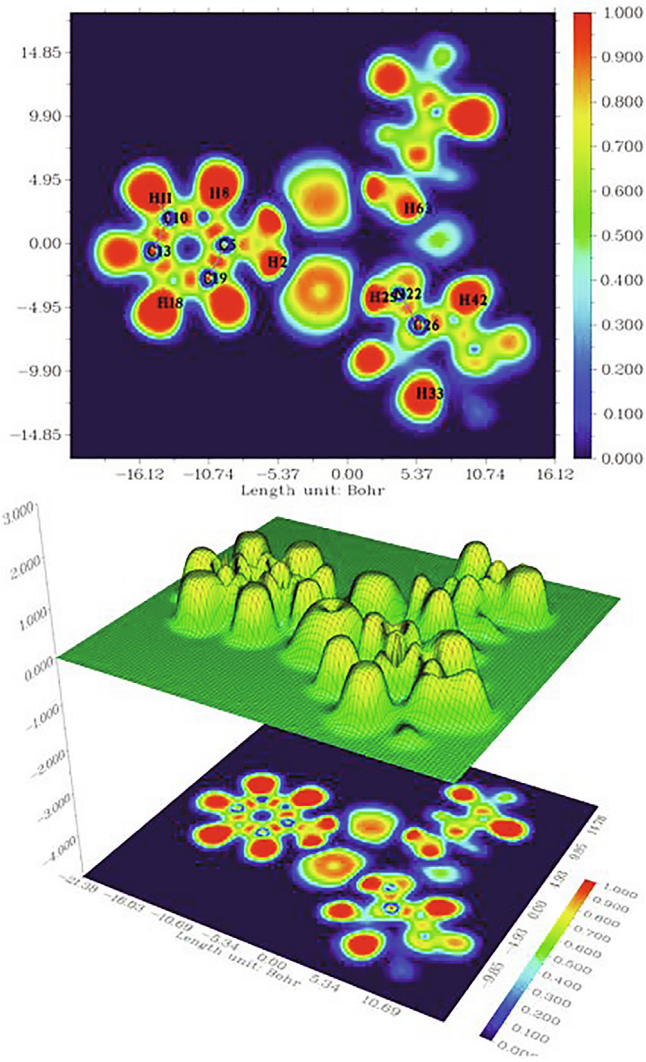

Fig. 7. Shaded surface plot with projection effect of ELF in XY plane of $(C_6H_{14}N)_3[CoCl_4]Cl$ compound.

pound were studied by IR spectroscopy to identify the functional groups present in the crystal and the assignment of the vibrational modes was performed by DFT calculation. The stability of the molecule was investigated by the TG/DTA thermal analysis. ESP method allows predicting the reactivity of the compound by investigating molecular interactions. Additionally, ELF presents single electron hydrogen atoms surrounded by the strongest regions with maximum Pauli repulsion, while the lowest regions with minimal Pauli repulsion are occupied by the chlorine atom of the tetrachlorocobaltate group and the carbon atoms of the organic entity.

Declaration of Competing Interest

The authors declare that they have no known competing financial interests or personal relationships that could have appeared to influence the work reported in this paper.

Acknowledgements

Researchers supporting project number (RSP-2021/61), King Saud University, Riyadh, Saudi Arabia.

Appendix A. Supplementary data

Supplementary data to this article can be found online at https://doi.org/10.1016/j.jksus.2021.101807.

References

Abkari, A., Chaabane, I., Guidara, K., 2017. Synthesis, crystal structure, Spectroscopic characterization and optical properties of bis(4-acetylanilinium) tetrachlorocobaltate(II). Phys. E 86, 210–217.

Akman F., Issaoui N., Kazachenko A.S., et al., 2020. Intermolecular hydrogen bond interactions in the thiourea/water complexes (Thio-$(H_2O)_n$) (n = 1, . . ., 5): X-ray, DFT, NBO, AIM, and RDG analyses. Journal of Molecular Modeling 26 (6).

Alvarez, S., Llunell, M., 2000. Continuous symmetry measures of penta-coordinate molecules: berry and non-Berry distortions of the trigonal bipyramid. J. Chem. Soc. 19, 3288–3303.

Arulraj, R., Sivakumar, S., Rajkumar, K., Jasinski, J.P., Kaur, M., Thiruvalluvar, A., 2020a. Synthesis, crystal structure, DFT calculations and Hirshfeld surface analysis of 3-chloro-3-methyl-r(2),c(6)-bis(p-methoxyphenyl)piperidin-4-one. J. Chem. Crystallogr. 50 (1), 41–51.

Arulraj, R., Sevgi, K., Necmi, D., Sivakumar, S., 2020b. Synthesis, Crystal Structure, DFT Calculations and Hirshfeld Surface Analysis of 3-Chloro-2,6-Bis(4-Chlorophenyl)-3-Methylpiperidin-4-One. J. Chem. Crystallogr. 50, 41–51.

Arulraj, R., Sivakumar, S., Suresh, S., Anitha, K., 2020c. Synthesis, vibrational spectra, DFT calculations, Hirshfeld surface analysis and molecular docking study of 3-chloro-3-methyl-2,6-diphenylpiperidin-4-one. Spectrochim. Acta A Mol. Biomol. Spectrosc. 232, 118166.

Arulraj, R., 2022. Hirshfeld surface analysis, interaction energy calculation and spectroscopical study of 3-chloro-3-methyl-r(2), c(6)-bis(p-tolyl)piperidin-4-one using DFT approaches. J. Mol. Struct. 1248, 131483.

Bader, R.F.W., Austen, M.A., 1997. Properties of atoms in molecules: atoms under pressure. J. Chem. Phys. 107 (11), 4271–4285.

Becke, A.D., 1993. Becke's three parameter hybrid method using the LYP correlation functional. J. Chem. Phys. 98, 5648–5652.

Brandenburg, K., 1998. Diamond Version 2.0 Impact, GbR, Bonn.

Bruker, 2006. APEX2. SAINT and SADABS, Bruker AXS Inc, Madison, Wisconsin, USA.

Chang, J.-C., Ho, W.-Y., Sun, I.-W., Chou, Y.-K., Hsieh, H.-H., Wu, T.-Y., 2011. Synthesis and proprieties of new tetrachlorocobaltate(II) and tetrachloromanganate(II) anion salts with dicationic counterions. Polyhedron 30, 497–507.

Chen, W.-Q., Feng, M.-H., Zhou, D.-D., Peng, Y.-Q., Han, S., Liu, X.-P., Yang, L.-M., Zhou, J.-R., Ni, C.-L., 2012. Two tetrachlorocobaltate(II) salts with substituted benzyl triphenylphosphonium: syntheses, crystal structures, weak interactions, and magnetic properties. Synth. React. Inorg. Met.-Org. Chem. 42 (6), 811–817.

Contreras-García, J., Yang, W., Johnson, E.R., 2011. Analysis of hydrogen-bond interaction potentials from the electron density: integration of noncovalent interaction regions. J. Phys. Chem. A 115 (45), 12983–12990.

Daghar, C., Issaoui, N., Roisnel, T., Dorcet, V., Marouani, H., 2021. Empirical and computational studies on newly synthesis cyclohexylammonium perchlorate. J. Mol. Struct. 1230, 129820.

Daghar, C., Issaoui, N., Marouani, H., Roisnel, T., Al-Dossary, O., 2022. Molecular structure, spectroscopy, quantum chemical and antibacterial activity investigations of 2-methylbenzylammonium perchlorate. J. Mol. Struct. 1247, 131311.

Dennington, R., Keith, T., Millam, J., 2009. GaussView, Version 5. Semichem, Inc, Mission, KS.

Essid, M., Roisnel, T., Rzaigui, M., Marouani, H., 2015. Synthesis, crystal structure, and characterization of a new non-centrosymmetric organic-inorganic hybrid material: $[C_6H_{16}N_2]_2$(BiBr 6)N_O3. Monatsh. Chem. 146 (12), 1959–1965.

Farrugia, L.J., 2012. WinGX and ORTEP for windows: an update. J. Appl. Cryst. 45 (4), 849–854.

Ferchichi, T., Trojett, B., Dhaouadi, H., Marouani, H., 2010. 1,4,8,11-Tetraazoniacyclotetradecane tetrachloridocobaltate(II) dichloride. Acta Crystallogr. 66 (8), m869–m870.

Frisch, M.J. et al., 2009. GAUSSIAN 09, Revision A.02. Gaussian Inc, Wallingford, CT.

Gatfaoui, S., Sagaama, A., Issaoui, N., Roisnel, T., Marouani, H., 2020. Synthesis, experimental, theoretical study and molecular docking of 1-ethylpiperazine-1,4-diium bis(nitrate). Solid State Sci. 106, 106326.

Gatfaoui S., Issaoui N., Brandán S.A., Medimagh M., Al-Dossary O., Roisnel T., Marouani H., Kazachenko A.S., et al., 2022. Deciphering non-covalent interactions of 1,3-Benzenedimethanaminium bis(trioxonitrate): Synthesis, empirical and computational study. Journal of Molecular Structure 1250, 131720.

Ghalla H., Issaoui N., Govindarajan M., Flakus H.T., Jamroz M.H., Oujia B., et al., 2014. Spectroscopic and molecular structure investigation of 2-furanacrylic acid monomer and dimer using HF and DFT methods. Journal of Molecular Structure 1059 (1), 132–143.

Humphrey, W., Dalke, A., Schulten, K., 1996. VMD-visual molecular dynamics. J. Mol. Graph. 14 (1), 33–38.

Jamróz, M.H., 2004. Vibrational Energy Distribution Analysis, vol. 4. Computer Program VEDA, Poland.

Jiang, L., Dong, H., Hu, W., 2010. Organic single crystal field-effect transistors: advances and perspectives. J. Mater. Chem. 20 (24), 4994.

Johnson, E.R., Keinan, S., Mori-Sánchez, P., Contreras-García, J., Cohen, A.J., Yang, W., 2010. Revealing Noncovalent Interactions. J. Am. Chem. Soc. 132 (18), 6498–6506.

Jomaa, I., Noureddine, O., Gatfaoui, S., Issaoui, N., Roisnel, T., Marouani, H., 2020. Experimental computational and in silico analysis of $(C_8H_{14}N_2)_2[CdCl_6]$ compound. J. Mol. Struct. 1213, 128186.

Jomaa, I., Issaoui, N., Roisnel, T., Marouani, H., 2021. Insight into non-covalent interactions in a tetrachlorocadmate salt with promising NLO properties: Experimental and computational analysis. J. Mol. Struct. 1242, 130730.

Kumar, P.S.V., Raghavendra, V., Subramanian, V., 2016. Bader's Theory of Atoms in Molecules (AIM) and its Applications to Chemical Bonding. J. Chem. Sci. 128 (10), 1527–1536.

Lu, T., Chen, F., 2012. Multiwfn: a multifunctional wavefunction analyzer. J. Comput. Chem. 33 (5), 580–592.

Moutia, N., Oueslati, A., Ben Gzaiel, M., Khirouni, K., 2016. Crystal structure and AC conductivity mechanism of $[N(C_3H_7)_4]_2CoCl_4$ compound. Physica E 83, 88–94.

Novena, L.M., Kumar, S.S., Athimoolam, S., 2016. Improved solubility and bioactivity of theophylline (a bronchodilator drug) through its new nitrate salt analyzed by experimental and theoretical approaches. J. Mol. Struct. 1116, 45–55.

Popelier, P.L.A., Aicken, F.M., O'Brien, S.E., 2000. Atoms in Molecules, an Introduction. Prentice Hall, 143–198.

D. Romani, O. Noureddine, N. Issaoui, S. A. Brandán, 2020. Properties and Reactivities of Niclosamide in Different Media, a Potential Antiviral to Treatment of COVID-19 by Using DFT Calculations and Molecular Docking. Biointerface Res. Appl. Chem. 10, 7295–7328.

Rozas, I., Alkorta, I., Elguero, J., 2000. Behavior of ylides containing N, O, and C atoms as hydrogen bond acceptors. J. Am. Chem. Soc. 122 (45), 11154–11161.

A. Sagaama, N. Issaoui, et al., 2020. Design, molecular docking analysis of an anti-inflammatory drug, computational analysis and intermolecular interactions energy studies of 1-benzothiophene-2-carboxylic acid. Comput. Biol. Chem. 88, 107348.

Sagaama A., Issaoui N., Al-Dossary O., Kazachenko A.S., Wojcik M.J., et al., 2021. Non covalent interactions and molecular docking studies on morphine compound. Journal of King Saud University - Science 33 (8), 101606.

Sheldrick, G.M., 2015a. SHELXT-integrated space-group and crystal-structure determination. Acta Cryst. 71 (1), 3–8.

Sheldrick, G.M., 2015b. Crystal structure refinement with SHELXL. Acta Crystallogr. C 71 (1), 3–8.

Tahenti, M., Gatfaoui, S., Issaoui, N., Roisnel, T., Marouani, H., 2020. A tetrachlorocobaltate(II) salt with 2-amino-5-picolinium: synthesis, theoretical and experimental characterization. J. Mol. Struct. 1207, 127781.

Wolff, S.K., Grimwood, D.J., McKinnon, J.J., Jayatilaka, D., Spackamn, M.A., 2013. Crystal Explorer 3.1. University of Westren Australia, Perth.

Yun, S.-S., Moon, H.-S., Kim, C.-H., Lee, S.-G., 2004. Synthesis and crystal structure of bis(dicyclohexylammonium) tetracyanonickel(II). J. Coord. Chem. 57 (1), 17–23.

Zheng, Y., Zhou, D.-D., Yu, L.-L., Han, S., Yang, L.-M., Liu, X.-P., Zhou, J.-R., Ni, C.-L., 2012. Syntheses, Crystal Structures and Antibacterial Properties of Bis(1-benzyl-4'-R-pyridinium) tetrabromocuprate(II) [R = NH_2 or $N(CH_3)_2$]. Synth. React. Inorg. Met.-Org. Chem. 42 (2), 238–245.

Zhou, P., Drumheller, J.E., Rubenacker, G.V., Halvorson, K., Willett, R.D., 1991. Novel low dimensional spin 1/2 antiferromagnets: Two-halide exchange pathways in A_2CuBr 4 salts. J. Appl. Phys. 69 (8), 5804–5806.

Further reading

Medimagh M., Issaou N., Gatfaoui S., Al-Dossary O., S. Kazachenko A., Marouani H., Wojcik M.J., et al., 2021. Molecular modeling and biological activity analysis of new organic-inorganic hybrid: 2-(3,4-dihydroxyphenyl) ethanaminium nitrate. Journal of King Saud University - Science 33 (8), 101616.